mater.scichina.com link.springer.com

Published online 29 November 2022 | https://doi.org/10.1007/s40843-022-2239-8
Sci China Mater 2023, 66(3): 982–991

Hierarchical porous separator with excellent isotropic modulus enabling homogeneous Zn^{2+} flux for stable aqueous Zn battery

Fenglin Zhang[1], Fanyang Huang[2], Renzhi Huang[1], Ning Dong[1], Shuhong Jiao[2], Ruiguo Cao[2] and Huilin Pan[1,3*]

ABSTRACT **Low-cost, high-safety aqueous Zn-ion batteries show promise for large-scale energy storage, but the unsatisfactory cycling stability of Zn anodes and the lack of a suitable hydrophilic separator for rechargeable aqueous Zn batteries limit their practical applications. In this work, we report a scalable method for the preparation of a homogenous polyvinylidene fluoride-lithium bistrifluoromethanesulfonimide (LiTFSI) (PVDF-Li)-based separator for aqueous Zn batteries. The homogenously mixed LiTFSI salt interrupted the crystalline framework of PVDF with excellent mechanical strength and led to hierarchical pore structures for the rapid and uniform Zn^{2+} flux through the separator. Meanwhile, the PVDF-Li separator exhibited excellent wettability toward aqueous Zn electrolytes. With the advanced PVDF-Li separator, the Zn dendrite growth can be suppressed greatly, showing an improved cycle life. The Zn||V_2O_5 full cell with PVDF-Li separator exhibited a 27% higher initial capacity (324 mA h g^{-1}) and considerably better capacity retention than the traditional glass fiber separator due to the uniform reaction on the V_2O_5 cathode and Zn anode sides. This work provides new insights into the development of high-performance aqueous batteries by regulating the reactions on the cathode and anode through functional separators.**

Keywords: aqueous Zn-ion battery, hierarchical porous separator, isotropic mechanical strength, dendrite growth suppression

INTRODUCTION

The development of new energy storage solutions with low cost and high safety is in high demand [1]. Among different battery chemistries, rechargeable aqueous Zn batteries have attracted paramount interest due to the advantages, such as low cost and high capacity of the Zn metal anode and their non-flammability [2,3]. However, the cycle life of aqueous Zn batteries is unsatisfactory in practice. This condition is mainly due to the formation of Zn dendrites and the occurrence of side reactions, such as corrosion and hydrogen generation [4]. Researchers have proposed a variety of methods to solve the above problems, such as the use of Zn electrodes with a three-dimensional structure [5,6], modification of the Zn electrode surface [7–11], and development of new electrolytes and additives [12–14]. The electrochemical performance of Zn anodes has been greatly improved with advanced Zn electrodes and electrolytes.

By contrast, the inactive components in aqueous Zn batteries have attracted notably less attention in spite of their importance in battery performance [15]. For example, the separator is a key component in batteries; it keeps the cathode and anode electrodes apart and controls the ion transportation and flux, which can modulate the Zn deposition behavior in an intensive way [16]. Therefore, Zn dendrites can be appropriately suppressed through advanced separators, which extend the cycle life of Zn batteries. Nevertheless, conventional polyolefin separators cannot work well in aqueous electrolytes due to their poor wettability. Glass fiber and cellulose membranes have been mainly used as separators in research due to the high wettability of aqueous electrolytes [17]. However, these separators have poor flexibility and tensile properties and large pores, and they lack the capability to inhibit Zn dendrite formation. Many improvements in glass fiber and cellulose separators have been reported; these enhancements include the addition of a coating on the surface [16,18,19], blending with ceramic particles [20], or improvement of the preparation method of the separator [21]. Recently, the proton exchange membrane Nafion film has been used as a separator in aqueous Zn batteries to promote the uniform distribution of charges on the Zn electrode and prevent the formation of Zn dendrites [22,23]. However, the low Young's modulus and high price of Nafion film may be inappropriate for practical use [24]. Hence, large-scale and low-cost aqueous battery separators with appropriate control of pore structure and mechanical strength must be developed to achieve high ionic conductivity and suppress Zn dendrite formation for long-life aqueous Zn batteries.

Here, we used polyvinylidene fluoride (PVDF) and lithium bistrifluoromethanesulfonimide (LiTFSI) as raw materials and prepared a well-mixed composite separator (PVDF-Li) with high ionic conductivity and potentially low cost. The PVDF-Li membrane was approximately 20 μm in thickness and exhibited excellent flexibility, mechanical strength, and surface flatness. The PVDF framework mixed with LiTFSI not only greatly improved the wettability of the aqueous Zn electrolyte but also generated hierarchical meso- and macro-pore structures for fast and smooth Zn^{2+} transport. Meanwhile, the PVDF-Li separator exhibited isotropic and excellent mechanical strength. The PVDF-Li separator promoted uniform and dense Zn deposition

[1] Department of Chemistry, Zhejiang University, Hangzhou 310027, China
[2] Department of Materials Science and Engineering, University of Science and Technology of China, Hefei 230026, China
[3] State Key Laboratory of Clean Energy Utilization, Zhejiang University, Hangzhou 310027, China
* Corresponding author (email: panhuilin@zju.edu.cn)

during repeated cycling, showing a stable interface at the Zn anode and an over five times longer cycle life of the Zn anode with a glass fiber separator. In addition, the Zn||V_2O_5 full cells demonstrated substantial improvement in achievable capacity and cycle life of 324 mA h g^{-1} at 0.5 A g^{-1} and 88% capacity retention over 475 cycles. This work provides useful insights into the design of advanced inactive components that play intensive active roles in determining the behavior of rechargeable metal batteries.

EXPERIMENTAL SECTION

Fabrication of separators

First, 0.85 g PVDF (HSV-900, purchased from Hefei Kejing) and 0.15 g LiTFSI (purchased from HIRONG Shandong) were added to 19 g *N*-methyl-2-pyrrolidone (NMP). After 24 h of stirring, a transparent solution can be obtained. Then, the solution was cast onto a glass plate using a doctor blade. The solvent was evaporated at 60°C for 12 h. Finally, the PVDF-Li separator with a thickness of ~20 μm was obtained. The separator can be easily peeled off from the glass plate at room temperature.

Preparation of V_2O_5 cathode

A total of 455 mg V_2O_5 (purchased from Macklin) and 2.5 mL H_2O_2 (30%) were dissolved in 42.5 mL distilled water. Then, the mixture was transferred to an autoclave and kept at 120°C for 10 h to obtain a brown solution. Water was removed after lyophilization, and the product was ground and dried at 60°C for 8 h. Subsequently, the V_2O_5 electrode was prepared by mixing the V_2O_5 powder, Super P, and PVDF at the mass ratio of 7:2:1 and casting the mixed slurry onto a carbon paper electrode. The mass loading of the active material was approximately 4 mg cm^{-2}.

Characterizations

The morphologies of separators and electrodes were analyzed by scanning electron microscopy (SEM, HITACHI SU8010 microscope), metallographic microscopy (CX40M-TRT), and atomic force microscopy (AFM, Dimension Icon, Bruker). The N_2 adsorption/desorption measurements of the PVDF-Li separator were conducted using a Micromeritics APSP 2460 analyzer. The crystalline phase, composition, and bond information of the samples were characterized using a Rigaku Ultima IV powder X-ray diffractometer (XRD) with Cu Kα radiation and a Renishaw inVia confocal Raman microscope. The Fourier transformed infrared spectroscopy (FTIR) was performed on a Thermofisher Nicolet iS50 in an attenuated total reflectance (ATR) mode. The thermostability was evaluated by a differential scanning calorimeter (DSC1/400, METTLER-TOLEDO), and the temperature range was from 40 to 260°C, with a heating rate of 10°C min^{-1}. The tensile property and electrolyte wettability of different separators were measured by an electronic testing machine (PARAM XLW) and contact angle meter (JY-82B Kruss DSA), respectively.

Electrochemical measurements

Coin cells (CR2032) were used for electrochemical measurements. Zn||Zn symmetric cells were assembled using Φ15 mm Zn foil (thickness: 30 μm, 99.9%, Yudingda) as both the working and counter electrodes. The 1 mol L^{-1} $Zn(TFSI)_2$ solution served as the aqueous electrolyte. $Zn(TFSI)_2$ (99.5% in purity) was purchased from Dado New Materials. Zn||Cu coin cells were used to evaluate the cycling stability and coulombic efficiency (CE) of the Zn metal with different separators with Cu (9 μm, MTI Corp) as the working electrode, Zn foil as the reference and counter electrode, and 1 mol L^{-1} $Zn(TFSI)_2$ solution as the electrolyte. The full cells were assembled by using V_2O_5 electrode as the cathode, Zn foil as the anode, and 3 mol L^{-1} $Zn(TFSI)_2$ as the aqueous electrolyte. Polypropylene (PP, Celgard 2400, 25 μm), glass fiber (Whatman GF/B, 675 μm), and PVDF-Li were used as the separators. Electrochemical impedance spectroscopy (EIS) measurements were carried out at the frequency range of 1 MHz to 1 Hz and a voltage amplitude of 10 mV for the separator conductivity and Zn||Zn symmetrical cells. Linear sweep voltammetry (LSV) tests for Zn||stainless steel (SS) cells were performed at a sweep speed of 0.5 mV s^{-1}. Chronoamperometry (CA) tests were used to measure the Zn^{2+} transference number with a constant potential of 20 mV. LSV, CA, and EIS measurements were conducted on a Bio-Logic VSP-300 multichannel electrochemical workstation.

Calculation of water uptake

Dried glass fiber and PVDF-Li separators were weighed to obtain W_{dry}. Then, they were immersed in distilled water for 0.5 h. The excess water was carefully wiped off, and W_{wet} was measured. The water uptake was calculated *via* Equation (1):

$$\text{Water uptake} = \frac{W_{wet} - W_{dry}}{W_{dry}} \times 100\%. \quad (1)$$

Calculation of Zn^{2+} transference number

The Zn^{2+} transference number was measured through CA and EIS tests on Zn||Zn symmetric cells and calculated using Equation (2):

$$t_{Zn^{2+}} = I_s(\Delta V - I_0R_0)/I_0(\Delta V - I_sR_s), \quad (2)$$

where I_0 and R_0 are the initial current and resistance, respectively. ΔV is the applied constant potential (20 mV), and I_s and R_s are the steady-state current and resistance, respectively [25].

RESULTS AND DISCUSSION

The PVDF-Li separator was prepared by a simple solution casting method, and the preparation process is shown in Fig. 1a. PVDF and LiTFSI (mass ratio 85:15) were mixed in NMP, and the solution was stirred for 24 h (solid content ratio: 5%). The PVDF-Li separator was obtained by casting the mixed solution onto a glass plate through a doctor blade (see details in the EXPERIMENTAL SECTION). The thickness of this separator was around 20 μm (Fig. S1), which is notably thinner than that of the commonly used glass fiber separator. The reduced length of the Zn^{2+} diffusion path facilitates the ion transport in aqueous Zn batteries [26]. The PVDF-Li separator showed a transparent and smooth surface, suggesting the even distribution of PVDF and LiTFSI in the film (Fig. 1b).

The physical and chemical characteristics of this separator were characterized in detail. XRD measurements showed that the diffraction peaks for PVDF and LiTFSI salts were greatly weakened in the PVDF-Li film (Fig. 1c), indicating the evidently reduced crystallinity of PVDF and LiTFSI [27]. The reduced crystallinity improved the uniformity and toughness of the separator and facilitated the transportation of Zn^{2+} through the separator. Compared with the pure PVDF membrane, the

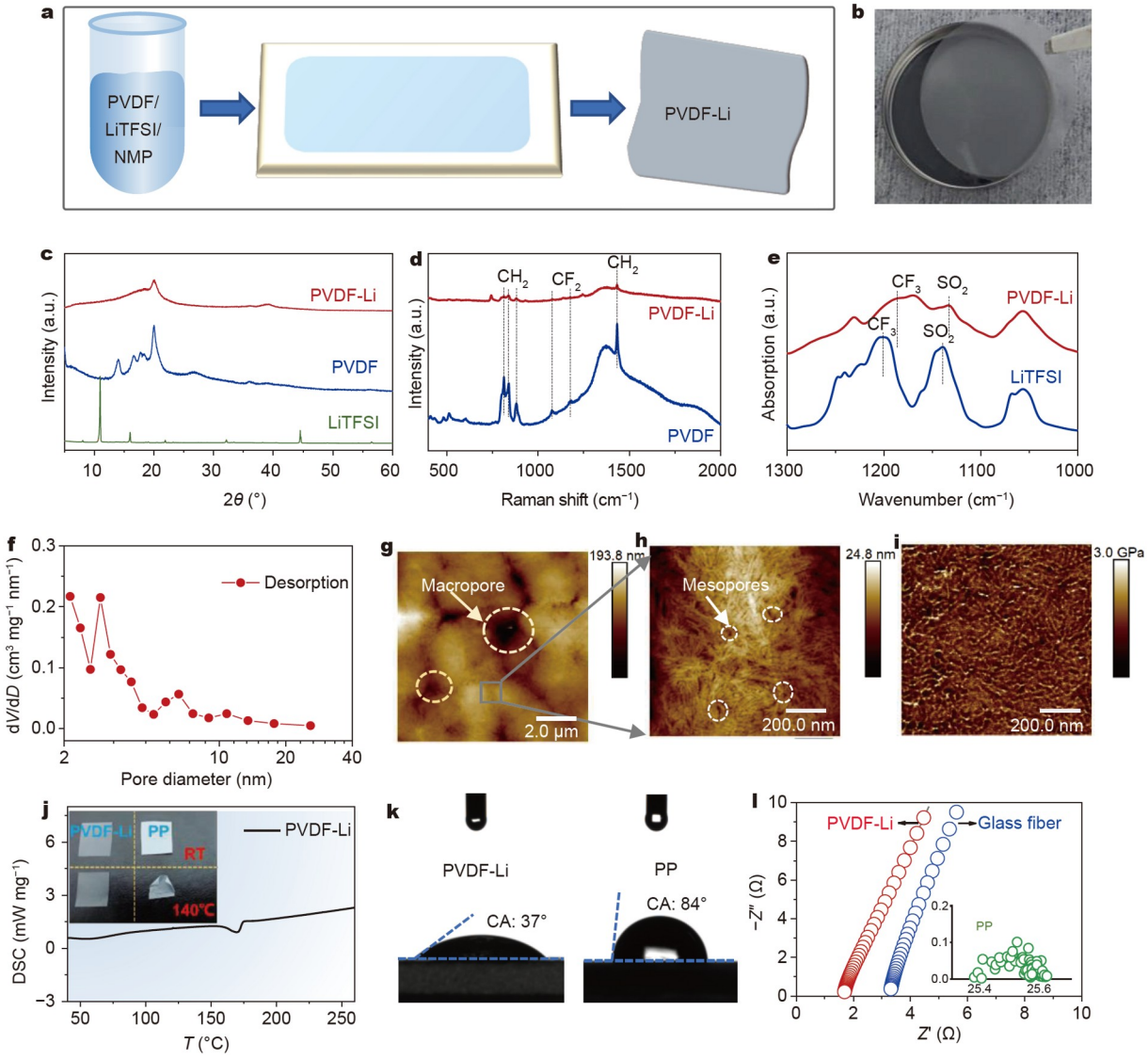

Figure 1 (a) Scheme of the fabrication process for the PVDF-Li separator. (b) Digital photo of a PVDF-Li film. (c) XRD patterns of the obtained PVDF-Li film, PVDF film, and LiTFSI salt. (d) Raman spectra of the obtained PVDF-Li and PVDF films. (e) FTIR spectra of the PVDF-Li film and LiTFSI. (f) BJH pore-size distributions of the PVDF-Li separator. (g, h) AFM images of the PVDF-Li membrane. (i) Modulus measurement of the PVDF-Li separator through Young's modulus mapping mode during the AFM. (j) DSC analysis of the PVDF-Li separator and comparison of the thermal shrinkages of PVDF-Li and PP separators at 140°C. (k) Wettability measurements of the PVDF-Li and commercial PP separator. (l) Nyquist plots for the symmetrical cells using SS as both the working and counter electrodes and commercial PP, glass fiber, and PVDF-Li films as the separators (electrolyte: 1 mol L^{-1} $Zn(TFSI)_2$ in H_2O).

PVDF-Li membrane presented broad Raman peaks of PVDF at 810, 837, 882, 1075, 1174, and 1432 cm^{-1} with greatly reduced intensity (Fig. 1d). These results further confirmed the uniform distribution of LiTFSI and reduced the crystallinity of the PVDF-Li membrane. FTIR was used to identify the interaction between salts and polymers (Fig. 1e). The vibration bands at 1200 and 1140 cm^{-1} corresponded to the stretching of CF_3 and SO_2 of the $TFSI^-$ anions, respectively, which exhibited a red shift in the PVDF-Li membrane, implying the potential interactions between PVDF and $TFSI^-$ anions. Such interactions can influence the ion transport through the separator (to be discussed later).

SEM, N_2 adsorption/desorption, and AFM measurements were employed to reveal the microscopic morphology and pore structure of the PVDF-Li separator (Fig. S2, Fig. 1f–i). The PVDF-Li membrane showed a flat surface with macropores (~2 μm) in the SEM image (Fig. S2a), which is similar to the image in the metallurgical microscopy (Fig. S2b). In addition, the AFM images further revealed the microscopic structure of the PVDF-Li membrane. As indicated in Fig. 1g and Fig. S3c, ~400 nm macropores connect the PVDF-Li particles in the film. The high-magnification AFM topographic image indicated a large number of 10–30 nm mesopores inside the PVDF-Li particles (Fig. 1h and Fig. S3d), suggesting the hierarchical pore structures of the film. Fig. S4a, b show the statistical distribution graphs for the macropores and mesopores in the SEM and AFM images of the PVDF-Li membrane. Barrett-Joyner-Halenda (BJH) pore-size distributions confirmed the formation of 2–30 nm nanopores in the PVDF-Li membrane (Fig. 1f). This pore structure of PVDF-Li evidently differed from that of

commercial polyolefin separators, such as the PP separator (Fig. S3a, b). The rich and hierarchical pore structures of the PVDF-Li separator can facilitate the transport of Zn^{2+} in the aqueous electrolytes while maintaining a smooth Zn^{2+} flux.

Young's modulus mapping of AFM was used to further reveal the mechanical properties of the PVDF-Li membrane (Fig. 1i and Fig. S5). The PVDF-Li membrane exhibited a high average modulus value of 1.9 GPa and isotropic distribution of modulus strength, and the PP separator showed an uneven distribution of modulus with an average of 0.9 GPa. Moreover, the elongation at break of the PVDF-Li separator was >50%, which was larger than that of the commercial PP separator (44% in the machine direction and 12% in the transverse direction) (Table S1). This finding suggested the excellent flexibility of the PVDF-Li membrane. The uniformly distributed pore structure, mechanical strength, and flexibility of the PVDF-Li separator can be helpful in the uniform and smooth Zn deposition. DSC test of the PVDF-Li membrane showed an absorption peak at approximately 170°C, which was assigned to the thermal decomposition of the PVDF-Li membrane (Fig. 1j). In addition, the PVDF-Li membrane exhibited a low thermal shrinkage rate compared with the commercial PP separator at 140°C, indicating the good thermal stability of the PVDF-Li membrane. These results proved that the PVDF-Li membrane is a good heat-resistant separator.

The PVDF-Li separator also showed significantly improved aqueous electrolyte wettability in comparison with the hydrophobic PP separator (Fig. 1k). The overall electrolyte uptake of the PVDF-Li separator can be significantly reduced (Fig. S6), which is beneficial to increasing the energy density of Zn batteries in practice [15]. It is worth noting that a good separator should enable excellent electrolyte wettability and ion transport with a reasonable electrolyte dosage. Among different separators, the PVDF-Li separator showed the smallest bulk resistance (Fig. 1l), which suggested the low ohmic resistance and fast Zn^{2+} transport through the PVDF-Li separator with an aqueous electrolyte. On the contrary, the impedance of the commercial PP separator with an aqueous electrolyte cannot be stabilized due to poor electrolyte wettability and contact. Therefore, the PP separator was not selected for comparison in the subsequent battery tests. The good wettability and low resistance of the PVDF-Li separator in aqueous electrolytes were closely related to the hydrophilic LiTFSI salt and rich pore structure of the film. In addition, LSV test was performed on Zn||SS cells using 1 mol L^{-1} $Zn(TFSI)_2$ as the electrolyte (Fig. S7). The PVDF-Li separator exhibited a similar electrochemical window up to 2.3 V *vs.* Zn. The CA method was used to estimate the transference number of Zn^{2+} ($t_{Zn^{2+}}$) through different separators. The PVDF-Li separator showed a $t_{Zn^{2+}}$ value of 0.71 (Fig. S8c), which was significantly higher than that of the glass fiber separator (0.47) (Fig. S8a). A high $t_{Zn^{2+}}$ favored the reduction of the concentration polarization of Zn^{2+} at the interface of the Zn anode during the Zn plating, which suppressed the formation of Zn dendrites at the Zn electrodes [21,28]. The high $t_{Zn^{2+}}$ in the PVDF-Li separator can be related to the interactions between the $TFSI^-$ anions and the PVDF framework, which enhanced the fast diffusion of Zn^{2+} cations.

To evaluate the influence of separators on the behavior of Zn plating/stripping, we assembled Zn||Cu cells and Zn||Zn symmetric cells using 1 mol L^{-1} $Zn(TFSI)_2$ as the electrolyte. Reversible galvanostatic discharge-charge technology for Zn||Cu cells was applied for CE measurement (Fig. 2a). The cycle life of Zn||Cu cells with the glass fiber separator was 66 h, which may be attributed to the low CE of ~80%. The Zn||Cu cell with the PVDF-Li separator showed improved cycling stability and high CE (~95%), which indicated that the PVDF-Li separator can promote uniform Zn plating/stripping to enhance the reversibility of the Zn anode [20]. Furthermore, the symmetrical Zn||Zn cell with the glass fiber separator quickly failed with a limited cycle life of ~240 h under 1 mA cm^{-2} and 1 mA h cm^{-2} (Fig. 2b). By contrast, the symmetrical Zn||Zn cell with a PVDF-Li separator showed a greatly improved cycle life of more than 1000 h, and a low polarization voltage of ~35 mV, which indicated the high reversibility of Zn plating/stripping with the PVDF-Li separator. Furthermore, under higher current density and areal capacity, the Zn||Zn cells with PVDF-Li separator still exhibited considerably better cycling stability than the traditional glass fiber separator (Fig. 2c, d). Stable cycling over 100 h, which was five times that of the glass fiber separator, can be reached for the Zn||Zn cell with a PVDF-Li separator under the condition of 5 mA cm^{-2} and 5 mA h cm^{-2}.

The transportation of Zn^{2+} slows down at low temperatures, which can lead to increased polarization voltage during Zn deposition and induce Zn dendrite growth at low temperatures [29,30]. The Zn||Zn symmetric cell with the designed PVDF-Li separator can still work normally at 0 and −10°C, with low polarizations of 33 and 43 mV, respectively, at 1 mA cm^{-2} and 1 mA h cm^{-2}. Meanwhile, the values for the glass fiber separator were 40 and 46 mV (Fig. 2e, g). The findings suggest that the new PVDF-Li separator broadens the application of aqueous Zn batteries in an extended temperature range without special treatment using an aqueous electrolyte. EIS was further determined to understand the interfacial Zn deposition kinetics and stability during the cycling (Fig. 2f, h). The Zn||Zn cells with a PVDF-Li separator showed a notably lower charge-transfer resistance in comparison with the traditional glass fiber separator. In addition, the resistance at the Zn anode with the PVDF-Li separator decreased continuously during cycling, suggesting that the PVDF-Li separator facilitated the fast Zn^{2+} ion transport at the interface. Meanwhile, the impedance on the Zn electrode with a glass fiber separator increased significantly from 50 to 100 cycles due to the accumulation of side reaction products [31,32]. This result was consistent with the early buildup of polarization and the limited cycle life of Zn||Zn cells with glass fiber separators.

To study the stability of the PVDF-Li separator during the cycling, we soaked the PVDF-Li separator in deionized water for four days to enhance the possible dissolution of LiTFSI salt. The element distribution on the surface of the soaked PVDF-Li separator was analyzed by X-ray energy dispersive spectroscopy (EDS) mapping (Fig. 3a). Nitrogen (N), oxygen (O), and sulfur (S) were still uniformly distributed in the separator after soaking and washing with water. Furthermore, to simulate the situation in the battery cycle, we tested the changes in the LiTFSI content when the PVDF-Li separator was soaked in the electrolyte (Fig. 3b). The sulfur content in PVDF-Li remained at around 3% after being immersed in the electrolyte for a long time. This result suggested that LiTFSI in the PVDF-Li separator can be mainly retained in the separator rather than being dissolved into the electrolyte during the battery cycling. We further tested the Zn||Zn cells with the glass fiber separator in an electrolyte with a

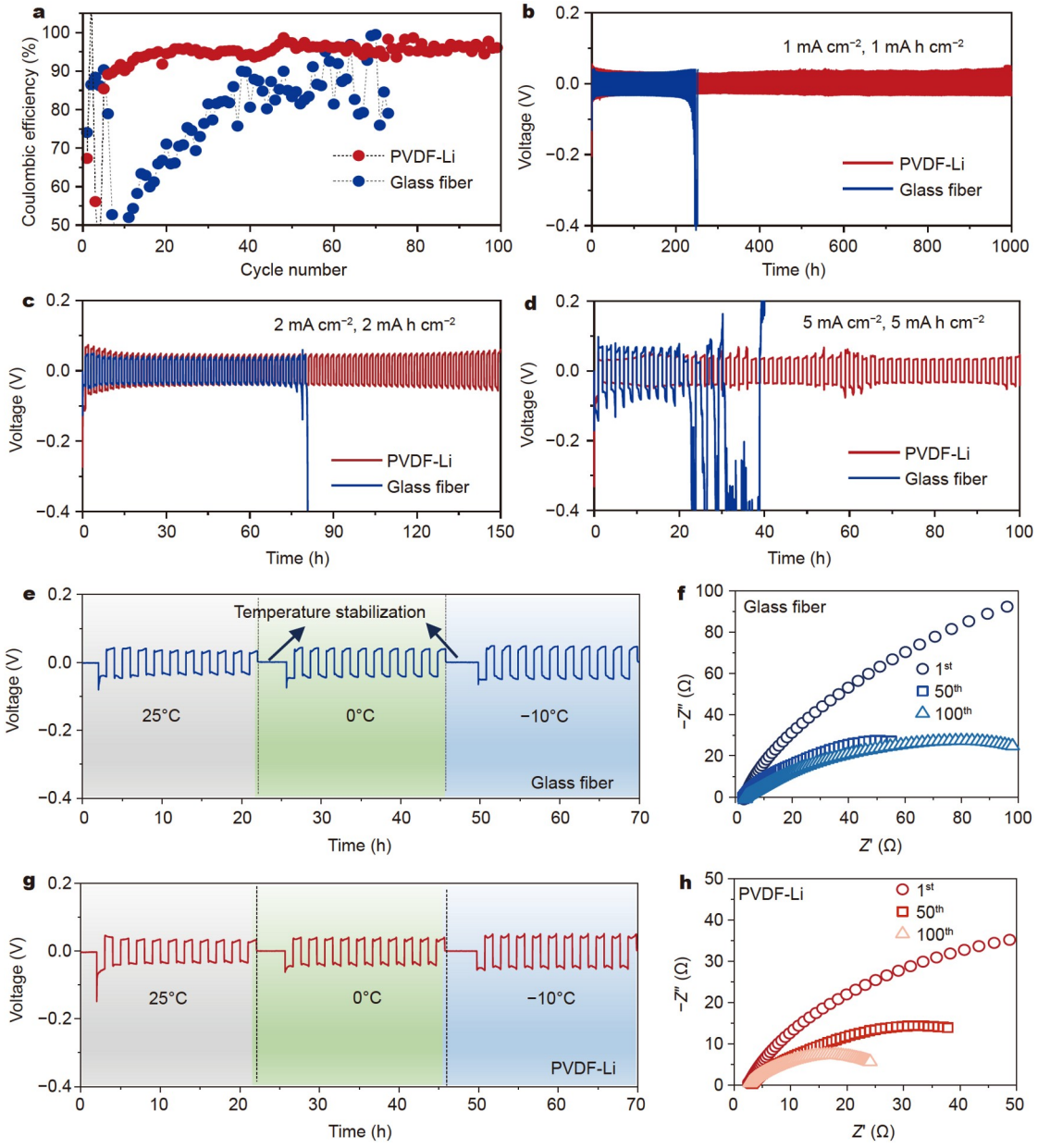

Figure 2 (a) CE characterization of the Zn||Cu cells using different separators under 1 mA cm^{-2} and 0.5 mA h cm^{-2}. Cycling stability of the Zn||Zn symmetrical cells using different separators under different conditions: (b) 1 mA cm^{-2} and 1 mA h cm^{-2}, (c) 2 mA cm^{-2} and 2 mA h cm^{-2}, (d) 5 mA cm^{-2} and 5 mA h cm^{-2}. (e, g) Low-temperature tests of Zn||Zn cells with different separators under 1 mA cm^{-2} and 1 mA h cm^{-2} (a resting process stabilized the temperature for variable-temperature tests). (f, h) Electrochemical impedance measurements for symmetrical Zn||Zn cells using glass fiber and PVDF-Li separators during cycling at 25°C. Zn (30 μm) was used for all experiments.

small amount of LiTFSI as an additive (Fig. 3c). The cycle life slightly decreased compared with the battery without the LiTFSI salt additive. This result indicated that the reason for the improved cell performance in Fig. 2 was mainly the use of the PVDF-Li separator rather than the dissolution of LiTFSI salt into the electrolyte. The LiTFSI salt in the PVDF-Li separator can significantly improve the hydrophilicity of the separator and thus facilitate Zn^{2+} diffusion through the separator. LiTFSI can also be replaced by other lithium salts, such as $LiCF_3SO_3$ (LiTFO) (Fig. 3d). In addition, the PVDF-Zn(TFSI)$_2$ separator can improve the cycle life of Zn (Fig. S9).

The morphologies of Zn electrodes with different separators were investigated during the cycling (Fig. 4 and Fig. S10). After 20 cycles, the Zn electrodes with the glass fiber separator exhibited a rough and loose deposition surface with a high surface area (Fig. 4a, b, and Fig. S10a, b). The Zn electrodes showed a coarse surface and large surface area, which resulted in additional side reactions and a large cell impedance. After 50 cycles, ~200 μm agglomerated Zn particles appeared on the surface of the Zn electrodes, showing a large number of cracks and powdery Zn deposition (Fig. 4e, f, and Fig. S10e, f). This phenomenon can be detrimental to the cycling stability of the Zn electrodes in rechargeable batteries. By contrast, the Zn electrodes with PVDF-Li separator exhibited a smooth, compact,

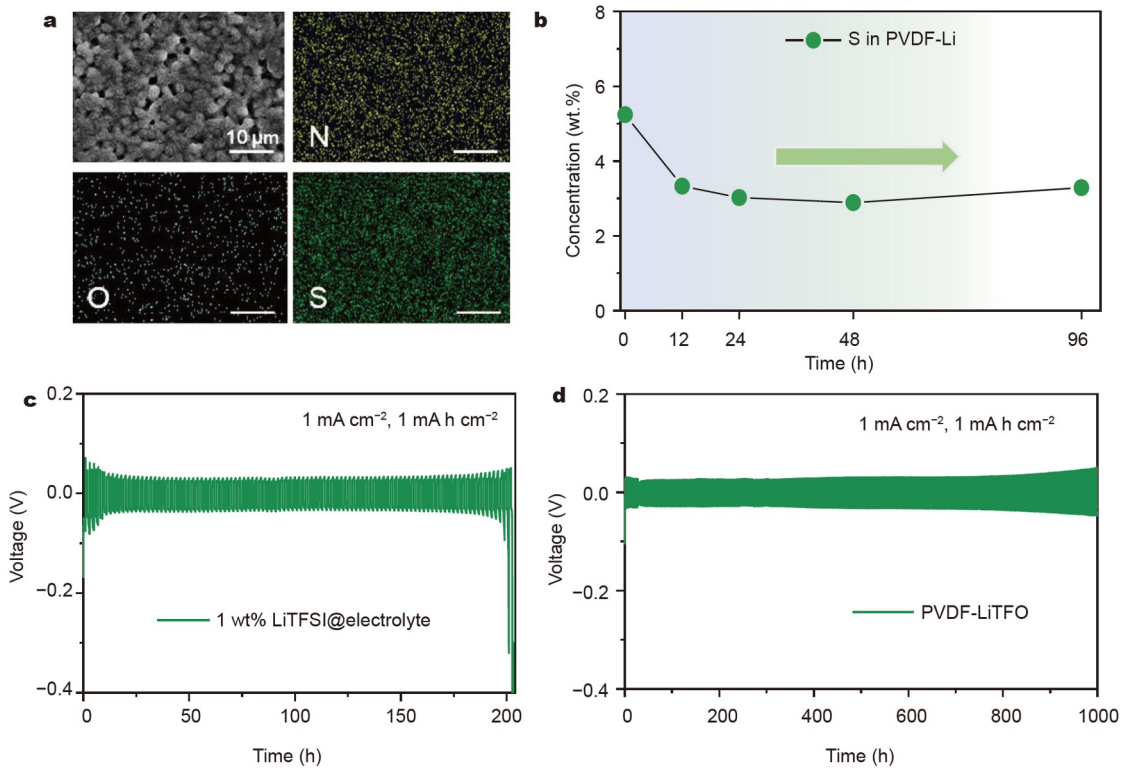

Figure 3 SEM imaging and EDS mapping of the PVDF-Li separator after water washing. (a) SEM images of the PVDF-Li separator and EDS mapping of N, O, and S on the surface. (b) S concentration in the PVDF-Li separator after soaking in 1 mol L^{-1} $Zn(TFSI)_2$ electrolyte for different periods (the soaked PVDF-Li separator was washed with deionized water before the EDS test). (c) Cycling stability of the Zn||Zn symmetrical cells with 1 mol L^{-1} $Zn(TFSI)_2$ + 1 wt% LiTFSI electrolyte using a glass fiber separator under 1 mA cm^{-2} and 1 mA h cm^{-2}. (d) Cycling stability of the Zn||Zn symmetrical cells with a PVDF-LiTFO separator under 1 mA cm^{-2} and 1 mA h cm^{-2}.

and dendrite-free morphology (Fig. 4c, d, and Fig. S10c, d). Furthermore, the homogenous Zn deposition morphology can be well retained during repeated cycles (Fig. 4g, h, and Fig. S10g, h). Fig. 4i, j show the digital photos of the Zn foils and separators after repeated cycles in Zn||Zn cells with two different separators. The glass fiber separator adhered to the Zn electrodes due to the powdery Zn deposition morphology and large pores of the glass fiber separator. Meanwhile, the Zn electrodes with a PVDF-Li separator showed a smooth and dense deposition layer, and the PVDF-Li separator almost retained its original feature. Notably, the PVDF-Li separator played an important role in enhancing the uniformity of Zn deposition and thus improving the cycle life of Zn electrodes.

The PVDF-Li separator was further studied in the Zn||V_2O_5 full cells. A high rate capability was considered a critical part of the application of aqueous Zn batteries in practice [33]. Compared with the glass fiber separator, the full cells using the PVDF-Li separator provided higher reversible capacity and capacity retention. Although the glass fiber separator typically exhibited considerably larger pores for Zn^{2+} diffusion through the separator, the full cell with PVDF-Li separator delivered a better rate performance than the glass fiber separator (Fig. 5a). This result suggested that the special pore structure of the PVDF-Li separator facilitated a smooth and fast Zn^{2+} diffusion compared with the conventional porous separator (to be discussed later). As depicted in Fig. 5b, the PVDF-Li full cell achieved a reversible capacity of 324 mA h g^{-1} at a current density of 0.5 A g^{-1}. Subsequently, the PVDF-Li separator enabled a super high CE of >99.95% and high capacity retention of 88% over 475 cycles for the Zn||V_2O_5 full cells. Meanwhile, the reversible capacity of the V_2O_5 electrode with the glass fiber separator can reach 254 mA h g^{-1} at the same current density of 0.5 A g^{-1}; the capacity started to fluctuate after 200 cycles and then quickly failed after about 246 cycles, and such a result can be caused by adverse intrinsic conductivity and blocked active sites [34,35]. Evident voltage fluctuations and decay in the charge-discharge curves can also be observed in the Zn||V_2O_5 full cells with the glass fiber separator (Fig. 5c). However, Zn||V_2O_5 full cells with the PVDF-Li separator showed almost overlapping charge-discharge curves during the cycling (Fig. 5d), which can be due to the enhanced uniformity of Zn deposition with the advanced PVDF-Li separator. Furthermore, the Zn||V_2O_5 full cells with the PVDF-Li separator presented a highly stable cyclic performance at 3 A g^{-1} with a remarkable capacity retention of 96.4% after 3000 cycles, exhibiting higher capacity and longer cycle lifespan than the glass fiber cells under the long-term high-rate cycling (Fig. S11).

The morphologies of electrodes and separators in Zn||V_2O_5 full cells were investigated further after 100 cycles. Fig. 5e shows the digital photos of cell components from the Zn||V_2O_5 full cells with glass fiber and PVDF-Li separators. The central part of the Zn electrode with the glass fiber separator was completely corroded with large holes. In addition, the powdery Zn and V_2O_5 electrodes adhered to the glass fiber separator due to the mossy Zn deposition morphology and poor mechanical stability of the glass fiber separator. For the full cell with the PVDF-Li

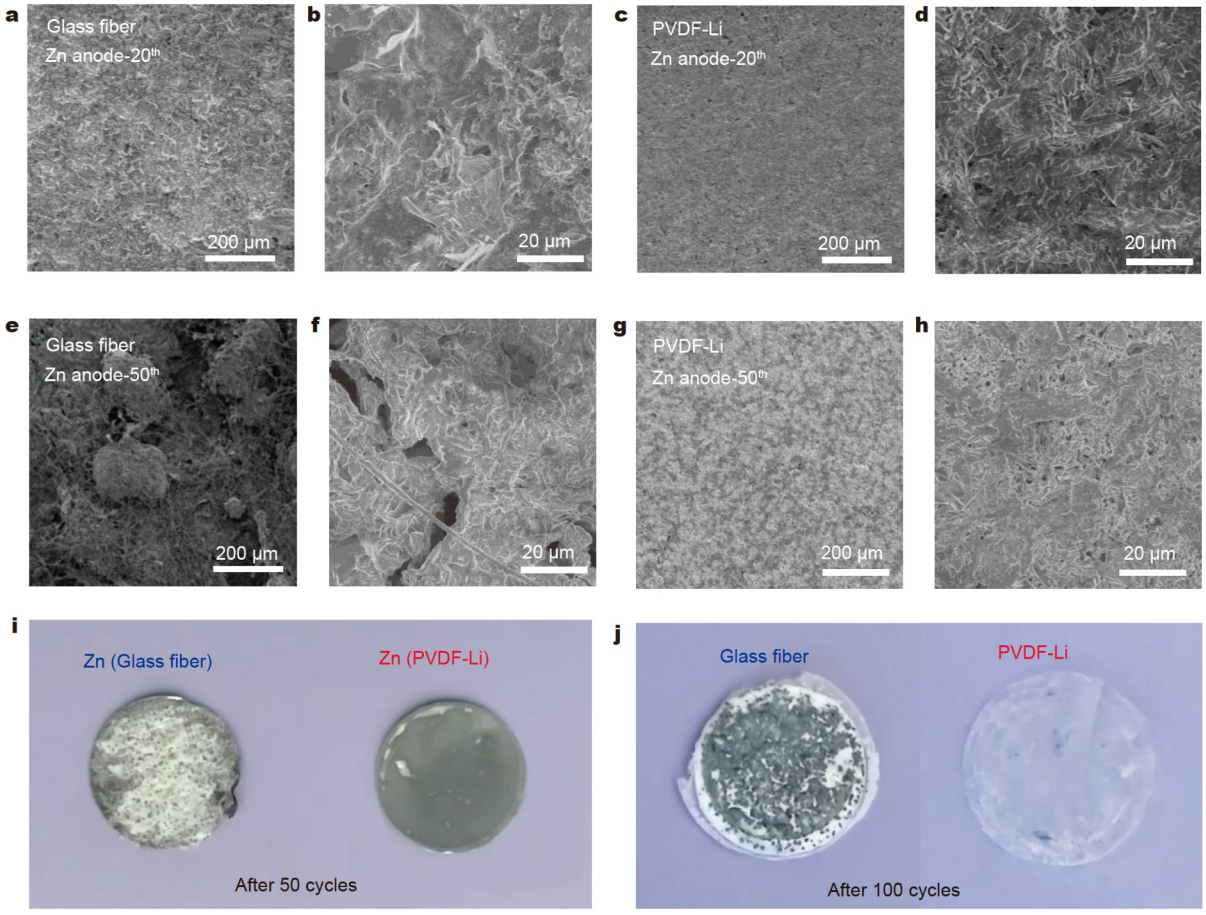

Figure 4 SEM images of Zn electrodes with different separators after various cycles: (a, b) glass fiber-20th, (c, d) PVDF-Li-20th, (e, f) glass fiber-50th, (g, h) PVDF-Li-50th. Digital photos of the Zn electrodes and corresponding separators after (i) 50 and (j) 100 cycles.

separator, the separator and V_2O_5 cathode remained smooth and flat with less difference from the original status before cell assembly. The morphology of the V_2O_5 cathodes after 100 cycles was examined further by SEM. Heterogenous and large aggregates of V_2O_5 particles were loosely distributed in the V_2O_5 cathode in the Zn||V_2O_5 full cell using a glass fiber separator (Fig. 5f and Fig. S12a). The uneven morphology of the V_2O_5 cathode was plausibly a copy of the nonuniform Zn deposition on the anode side, which was observed in rechargeable Li metal batteries [36]. By contrast, the V_2O_5 cathode with the PVDF-Li separator retained a flat and smooth surface (Fig. 5g and Fig. S12b). The shape of the Zn anode can be well retained after 100 cycles, showing a uniform deposition layer on the Zn electrode (Fig. 5h and Fig. S12c). The enhanced reversible capacity and cycling stability of Zn||V_2O_5 full cells can be ascribed to the uniform and reversible reactions on the V_2O_5 cathode and Zn anode sides, which results from the use of the PVDF-Li separator.

Fig. 6 further presents the function of separators in rechargeable aqueous Zn batteries. Glass fiber separators are typically composed of randomly distributed microfibers with an irregular pore size of ~1 μm [37]. These large pores are prone to causing rough and loose Zn deposition (Fig. 6a). The mossy Zn deposition can easily generate Zn dendrites, which penetrate the large pores of glass fiber separators and lead to more side reactions due to the increased surface area of the Zn deposition layer [38–40]. In comparison with the typical porous separator, the PVDF-Li separator consisted of homogenously distributed PVDF-Li clusters with a primary pore size of 100–400 nm, and rich secondary pores (2–30 nm) existed inside each PVDF-Li cluster (Fig. 1f–h, and Fig. 6b). Recently, this strategy of using hierarchical pores to regulate the uniform deposition of ions has been investigated for Li metal batteries [41]. The homogenously mixed PVDF-Li separator showed excellent wettability toward aqueous electrolytes due to the existence of LiTFSI salt (Fig. 1k). The PVDF-Li separator can quickly absorb aqueous electrolytes and enable the fast and homogenous Zn^{2+} diffusion through the rich and hierarchical pore structure of the separator. Therefore, smooth and compact Zn deposition can be achieved in the cell with the PVDF-Li separator, which was consistent with the greatly improved stability and utilization of the Zn anode (Fig. 5). In addition, the PVDF-Li separator showed high Young's modulus and isotropic machinal strength, which also enhanced the homogenous Zn deposition. After long cycling of the battery, Zn and the glass fiber separator attached to each other, which caused difficulty in observing the deposition morphology on the Zn surface. The PVDF-Li separator can maintain a smooth surface during long-term cycling, which is important in the study of Zn deposition behaviors of Zn batteries.

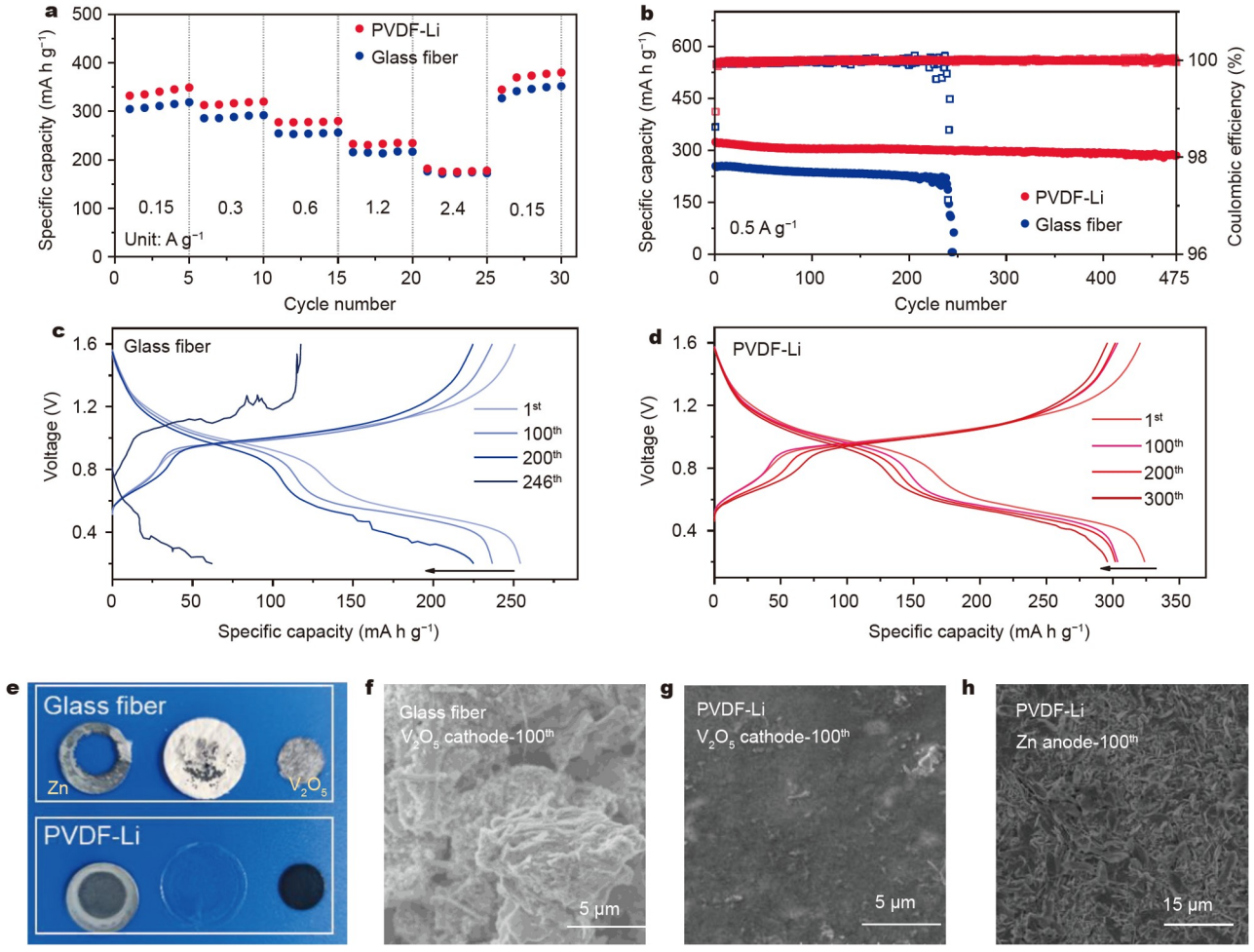

Figure 5 (a) Rate performance of the Zn||V_2O_5 full cells with different separators. (b) Cycling stability of the Zn||V_2O_5 full cells with different separators at 0.5 A g^{-1}. (c, d) Galvanostatic charge-discharge profiles of the Zn||V_2O_5 full cells at 0.5 A g^{-1} using the glass fiber and PVDF-Li separators, respectively. (e) Digital photos of the cell components of Zn anodes, separators, and V_2O_5 cathodes of the full cells after 100 cycles at 0.5 A g^{-1} with two different separators. SEM images of V_2O_5 cathodes after 100 cycles at 0.5 A g^{-1} with (f) glass fiber and (g) PVDF-Li separators. (h) SEM image of the Zn anode after 100 cycles with the PVDF-Li separator.

An appropriate design of aqueous separators is important to improve the performance and achievable energy density of the cells. The wettability and mechanical strength of electrolytes should be well considered to gain good ion conduction and prevent short circuits. At present, the most commonly used glass fiber separator has high porosity and good wettability due to randomly stacked fibers. However, the growth of dendrites is hard to suppress, given the poor mechanical properties of such separators. Furthermore, a high pore density is beneficial to improving the uniformity of Zn deposition [37], and a large pore size can reduce the overpotential during Zn deposition [42]. The pore density and average pore size of the separator are difficult to increase simultaneously while maintaining mechanical strength. A hierarchical porous separator considers both to a certain extent, thus providing an approach for regulating and enhancing the Zn^{2+} flux with fast kinetics spontaneously and favoring the stable cycling of aqueous Zn batteries. Importantly, the cost of the PVDF-Li separator can be potentially low due to its very light weight and simple fabrication method, which are evident advantages over glass fibers and commercial polyolefin membranes. Currently, the PVDF-Li separator is more suitable for aqueous electrolytes with sulfonate-based Zn salts, such as $Zn(TFSI)_2$ and $Zn(OTf)_2$. Future development of high-performance aqueous separators for common aqueous electrolytes with sulfate-based salts, such as $ZnSO_4$, can also be important.

CONCLUSION

In summary, we have designed an advanced hydrophilic PVDF-Li composite separator toward stable Zn anodes with suppressed Zn dendrite formation. Different from the conventional porous separators, the PVDF-Li separator consisted of Zn^{2+} ions-conducting clusters with rich and hierarchical pore structures and excellent isotropic mechanical strength. The special pore structure of the PVDF-Li separator led to homogenous Zn^{2+} diffusion and enhanced fast Zn^{2+} flux across the separator, which enabled a smooth and compact Zn deposition with excellent reaction kinetics. The Zn anode with the PVDF-Li separator delivered a cycle life five times longer than the Zn anode with a conventional glass fiber separator. In addition, the Zn||V_2O_5 full cells with the PVDF-Li separator provided a greatly improved reversible capacity of the V_2O_5 cathodes and cycling stability of the full cells, showing a good capacity retention of 88% after 475

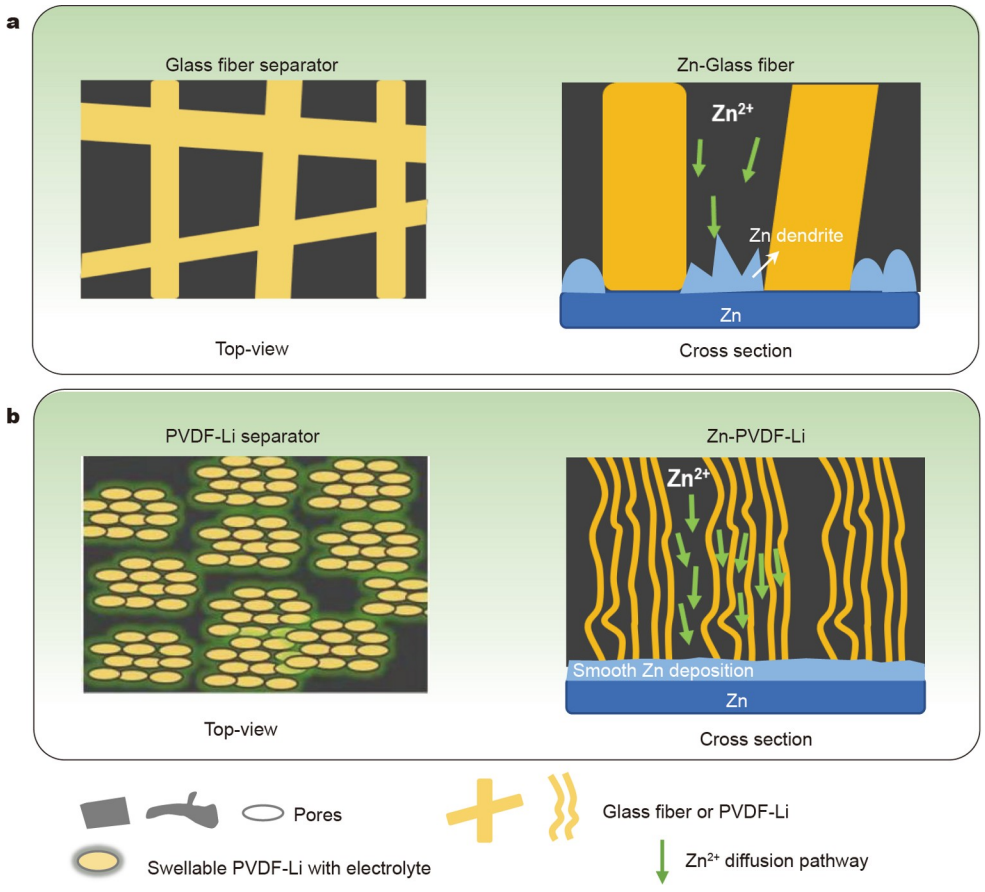

Figure 6 Schematics of different separators for Zn^{2+} transportation and Zn deposition behaviors. (a) Glass fiber separator; (b) PVDF-Li separator.

cycles at 0.5 A g^{-1} and significantly high CE of 99.95%. The PVDF-Li separator can also be prepared by a simple and inexpensive method with well-controlled thickness and flexibility compared with the glass fiber separator, which can be helpful in improving the energy density and reliability of rechargeable aqueous batteries. We believe that this high-efficiency and cost-efficient separator can provide insights into the development of high-performance aqueous batteries for safe and low-cost energy storage solutions.

Received 28 June 2022; accepted 30 August 2022; published online 29 November 2022

1 Chu S, Majumdar A. Opportunities and challenges for a sustainable energy future. Nature, 2012, 488: 294–303
2 Tang B, Shan L, Liang S, *et al.* Issues and opportunities facing aqueous zinc-ion batteries. Energy Environ Sci, 2019, 12: 3288–3304
3 Jia H, Wang Z, Tawiah B, *et al.* Recent advances in zinc anodes for high-performance aqueous Zn-ion batteries. Nano Energy, 2020, 70: 104523
4 Yan C, Li HR, Chen X, *et al.* Regulating the inner Helmholtz plane for stable solid electrolyte interphase on lithium metal anodes. J Am Chem Soc, 2019, 141: 9422–9429
5 Zhang Q, Luan J, Fu L, *et al.* The three-dimensional dendrite-free zinc anode on a copper mesh with a zinc-oriented polyacrylamide electrolyte additive. Angew Chem Int Ed, 2019, 58: 15841–15847
6 Priecel P, Lopez-Sanchez JA. Advantages and limitations of microwave reactors: From chemical synthesis to the catalytic valorization of bio-based chemicals. ACS Sustain Chem Eng, 2019, 7: 3–21
7 Liang P, Yi J, Liu X, *et al.* Highly reversible Zn anode enabled by controllable formation of nucleation sites for Zn-based batteries. Adv Funct Mater, 2020, 30: 1908528
8 Zhao Z, Zhao J, Hu Z, *et al.* Long-life and deeply rechargeable aqueous Zn anodes enabled by a multifunctional brightener-inspired interphase. Energy Environ Sci, 2019, 12: 1938–1949
9 Zhou Z, Zhang Y, Chen P, *et al.* Graphene oxide-modified zinc anode for rechargeable aqueous batteries. Chem Eng Sci, 2019, 194: 142–147
10 Xie D, Wang ZW, Gu ZY, *et al.* Polymeric molecular design towards horizontal Zn electrodeposits at constrained 2D Zn^{2+} diffusion: Dendrite-free Zn anode for long-life and high-rate aqueous zinc metal battery. Adv Funct Mater, 2022, 32: 2204066
11 Wang M, Meng Y, Li K, *et al.* Toward dendrite-free and anti-corrosion Zn anodes by regulating a bismuth-based energizer. eScience, 2022, 2: 509–517
12 Wang F, Borodin O, Gao T, *et al.* Highly reversible zinc metal anode for aqueous batteries. Nat Mater, 2018, 17: 543–549
13 Zhao J, Zhang J, Yang W, *et al.* "Water-in-deep eutectic solvent" electrolytes enable zinc metal anodes for rechargeable aqueous batteries. Nano Energy, 2019, 57: 625–634
14 Yan M, Xu C, Sun Y, *et al.* Manipulating Zn anode reactions through salt anion involving hydrogen bonding network in aqueous electrolytes with PEO additive. Nano Energy, 2021, 82: 105739
15 Ni Q, Kim B, Wu C, *et al.* Non-electrode components for rechargeable aqueous zinc batteries: Electrolytes, solid-electrolyte-interphase, current collectors, binders, and separators. Adv Mater, 2022, 34: 2108206
16 Li C, Sun Z, Yang T, *et al.* Directly grown vertical graphene carpets as Janus separators toward stabilized Zn metal anodes. Adv Mater, 2020, 32: 2003425
17 Xu W, Wang Y. Recent progress on zinc-ion rechargeable batteries. Nano-Micro Lett, 2019, 11: 90
18 Hou Z, Gao Y, Tan H, *et al.* Realizing high-power and high-capacity

zinc/sodium metal anodes through interfacial chemistry regulation. Nat Commun, 2021, 12: 3083
19 Liu T, Hong J, Wang J, *et al.* Uniform distribution of zinc ions achieved by functional supramolecules for stable zinc metal anode with long cycling lifespan. Energy Storage Mater, 2022, 45: 1074–1083
20 Cao J, Zhang D, Gu C, *et al.* Modulating Zn deposition *via* ceramic-cellulose separator with interfacial polarization effect for durable zinc anode. Nano Energy, 2021, 89: 106322
21 Zhou W, Chen M, Tian Q, *et al.* Cotton-derived cellulose film as a dendrite-inhibiting separator to stabilize the zinc metal anode of aqueous zinc ion batteries. Energy Storage Mater, 2022, 44: 57–65
22 Wu B, Wu Y, Lu Z, *et al.* A cation selective separator induced cathode protective layer and regulated zinc deposition for zinc ion batteries. J Mater Chem A, 2021, 9: 4734–4743
23 Yuan D, Manalastas Jr. W, Zhang L, *et al.* Lignin@Nafion membranes forming Zn solid-electrolyte interfaces enhance the cycle life for rechargeable zinc-ion batteries. ChemSusChem, 2019, 12: 4889–4900
24 He SS, Strickler AL, Frank CW. A semi-interpenetrating network approach for dimensionally stabilizing highly-charged anion exchange membranes for alkaline fuel cells. ChemSusChem, 2015, 8: 1472–1483
25 Ma L, Li Q, Ying Y, *et al.* Toward practical high-areal-capacity aqueous zinc-metal batteries: Quantifying hydrogen evolution and a solid-ion conductor for stable zinc anodes. Adv Mater, 2021, 33: 2007406
26 Fang Y, Xie X, Zhang B, *et al.* Regulating zinc deposition behaviors by the conditioner of PAN separator for zinc-ion batteries. Adv Funct Mater, 2022, 32: 2109671
27 Liu W, Yi C, Li L, *et al.* Designing polymer-in-salt electrolyte and fully infiltrated 3D electrode for integrated solid-state lithium batteries. Angew Chem Int Ed, 2021, 60: 12931–12940
28 Yan H, Li S, Nan Y, *et al.* Ultrafast zinc-ion-conductor interface toward high-rate and stable zinc metal batteries. Adv Energy Mater, 2021, 11: 2100186
29 Born F. R. S. M, Green HS. A kinetic theory of liquids. Nature, 1947, 159: 251–254
30 Zhao Y, Chen Z, Mo F, *et al.* Aqueous rechargeable metal-ion batteries working at subzero temperatures. Adv Sci, 2021, 8: 2002590
31 Xiao J, Li Q, Bi Y, *et al.* Understanding and applying coulombic efficiency in lithium metal batteries. Nat Energy, 2020, 5: 561–568
32 Guan X, Wang A, Liu S, *et al.* Controlling nucleation in lithium metal anodes. Small, 2018, 14: 1801423
33 Chuai M, Yang J, Wang M, *et al.* High-performance Zn battery with transition metal ions co-regulated electrolytic MnO_2. eScience, 2021, 1: 178–185
34 Ruan P, Liang S, Lu B, *et al.* Design strategies for high-energy-density aqueous zinc batteries. Angew Chem Int Ed, 2022, 61: e202200598
35 Heng Y, Gu Z, Guo J, *et al.* Research progresses on vanadium-based cathode materials for aqueous zinc-ion batteries. Acta Physico Chim Sin, 2020, 0: 2005013–0
36 Pan H, Han KS, Engelhard MH, *et al.* Addressing passivation in lithium-sulfur battery under lean electrolyte condition. Adv Funct Mater, 2018, 28: 1707234
37 Qin Y, Liu P, Zhang Q, *et al.* Advanced filter membrane separator for aqueous zinc-ion batteries. Small, 2020, 16: 2003106
38 Wu S, Chen Y, Jiao T, *et al.* An aqueous Zn-ion hybrid supercapacitor with high energy density and ultrastability up to 80 000 cycles. Adv Energy Mater, 2019, 9: 1902915
39 Wu B, Lochala J, Taverne T, *et al.* The interplay between solid electrolyte interface (SEI) and dendritic lithium growth. Nano Energy, 2017, 40: 34–41
40 Zhang Y, Yang G, Lehmann ML, *et al.* Separator effect on zinc electrodeposition behavior and its implication for zinc battery lifetime. Nano Lett, 2021, 21: 10446–10452
41 Wang J, Liu Y, Cai Q, *et al.* Hierarchically porous silica membrane as separator for high-performance lithium-ion batteries. Adv Mater, 2022, 34: 2107957
42 Ghosh M, Vijayakumar V, Kurungot S. Dendrite growth suppression by Zn^{2+}-integrated Nafion ionomer membranes: Beyond porous separators toward aqueous Zn/V_2O_5 batteries with extended cycle life. Energy Technol, 2019, 7: 1900442

Acknowledgements This work was supported by the National Natural Science Foundation of China (22179117 and U21A2075) and the startup foundation for the Hundred-Talent Program of Zhejiang University. XRD and SEM measurements were performed at the Chemistry Instrument Center, Department of Chemistry, Zhejiang University. AFM was performed at the University of Science and Technology of China.

Author contributions Zhang F conducted the experiment; Huang F, Jiao S and Cao R performed the AFM measurement. Huang R and Dong N performed some data analysis and offered helpful suggestions. Zhang F and Pan H designed this study, analyzed the data and wrote the paper. All authors contributed to the general discussion.

Conflict of interest The authors declare that they have no conflict of interest.

Supplementary information Supporting data are available in the online version of the paper.

Fenglin Zhang received his BS degree in chemistry from Xiamen University in 2020. He then joined the Department of Chemistry at Zhejiang University under the supervision of Prof. Huilin Pan. His research focuses on the design of new electrolytes and separators for energy storage devices.

Huilin Pan is a group leader for the energy storage material research at the Department of Chemistry, Zhejiang University. She received her PhD degree in condensed matter physics from the Institute of Physics, Chinese Academy of Sciences in 2013. In the past, she worked as a staff scientist at Pacific Northwest National Laboratory. Her research interest is primarily engaged in new energy storage battery materials and systems, including rechargeable aqueous Zn batteries, Na-ion batteries, and solid electrolyte interphases.

各向同性模量的分级多孔隔膜促进锌离子均匀扩散及水系锌离子电池循环稳定性

张丰麟[1], 黄凡洋[2], 黄仁智[1], 董宁[1], 焦淑红[2], 曹瑞国[2], 潘慧霖[1,3*]

摘要 水系锌离子电池具有低成本、高安全的特点，有望应用于大规模储能. 然而，锌负极的循环稳定性仍不理想，且水系电池缺少合适的亲水隔膜，这限制了水系锌离子电池的实际应用. 在本文中，我们报道了一种可用于水系电池的分级多孔的聚偏二氟乙烯-双三氟甲磺酰亚胺锂(PVDF-LiTFSI) (PVDF-Li)隔膜. 均匀混合的LiTFSI盐降低了PVDF的结晶性，使隔膜具有优异的机械强度，并形成分级的孔隙结构. 这种LiTFSI诱导的分级多孔结构有助于实现Zn^{2+}的快速传输和锌的均匀沉积，同时保证隔膜在水系电解液中具有优异的润湿性. 这种先进的PVDF-Li隔膜能显著抑制锌枝晶的生长，提高水系锌离子电池的循环寿命. 因此，使用PVDF-Li隔膜的$Zn||V_2O_5$电池的初始容量达324 mA h g^{-1}，比传统玻璃纤维隔膜高27%，且容量保持率也得到大幅提升. 该研究设计了一种功能隔膜来调控正负极反应的均匀性，这为高性能水系电池的开发提供了新的思路.

